*J. Electrochem. Sci. Eng.* **12(4)** (2022) 767-776; https://dx.doi.org/10.5599/jese.1458

Open Access : : ISSN 1847-9286
https://pub.iapchem.org/ojs/index.php/JESE

*Original scientific paper*

# Influence of operating temperature on the activation efficiency of Li-ion cells with $xLi_2MnO_3$-(1-x)$LiMn_{0.5}Ni_{0.5}O_2$ electrodes

Renny Nazario-Naveda[1,✉], Segundo Rojas-Flores[2], Moises Gallozzo-Cardenas[3], Luisa Juárez-Cortijo[4] and Luis Angelats-Silva[5]

[1]*Universidad Autónoma del Perú, Lima, Perú*
[2]*Universidad Señor de Sipán, Chiclayo, Perú*
[3]*Universidad César Vallejo, Trujillo, Perú*
[4]*Universidad Privada del Norte, Trujillo, Perú*
[5]*Universidad Privada Antenor Orrego, Trujillo, Perú*

*Corresponding author:* ✉*scored731@gmail.com; Tel.: +51-951-344-316*

Received: July 15, 2022; Accepted: September 3, 2022; Published: September 12, 2022

***Abstract***

*In this study, the effect of operating temperature at 55 °C on $xLi_2MnO_3$-(1-x)$LiMn_{0.5}Ni_{0.5}O_2$ electrodes during the charge/discharge process at different current densities was investigated. X-ray diffraction (XRD) and scanning electron microscopy (SEM) were used for structural and morphological analysis of the fabricated cathode materials, while charge-discharge curves and differential capacity were used to study the electrochemical behavior. Results confirm the formation of the structures with two phases associated with the components of the layered material. It was found that at 55 °C, a capacity higher than 357 mAh $g^{-1}$ could be achieved at a voltage of 2.5-4.8 V vs. $Li/Li^+$, which was larger than the capacity achieved at room temperature. At 55 °C, a change in valence could be observed during charging and discharging due to the change in the position of the peaks associated with Mn and Ni, highlighting cathodic material with x = 0.5 as the material that retains the layered structure at this temperature. This work confirms the good performance of electrodes made with this material at elevated temperatures and gives a better understanding of its electrochemical behavior.*

**Keywords**

Lithium-ion battery; cathode material; Li-rich Mn-Ni oxide; operating temperature; specific capacity

## Introduction

In the 21st century, energy and the environment are fundamental issues for human survival and social development [1]. Several industrial applications require rechargeable batteries working at elevated temperatures, such as the power supply of electric vehicles [2]. For such particular

applications, batteries are exposed to an operating temperature range of 20 to 50 °C and should be able to undergo only moderate degradations at those temperatures. Rechargeable lithium-ion batteries are good candidates for such applications [3-5].

Many combinations of positive and negative electrodes have already been tested, graphite or $Li_4Ti_5O_{12}$ materials for the negative electrode, and $LiMn_2O_4$, $LiCoO_2$ or $LiFePO_4$ materials for the positive electrode [6,7]. However, in recent years there has been a growing interest in the layered $xLi_2MnO_3$–$(1-x)LiMO_2$ (M = Mn, Ni) (LMO) oxides as positive electrode materials for lithium-ion batteries due to their good electrochemical properties and better thermal stability in the charged state [8,9]. These good properties are mainly related to the presence of Ni at a divalent state and to a large amount of stable $Mn^{4+}$ cations playing a stabilizing role of the structure, especially in the charged state of batteries. Also, the excess of Li can be easily incorporated into the layered structure through the integration of $Li_2MnO_3$ in $LiMO_2$, substituting transition metals M [10].

Commercial lithium-ion batteries manufactured today are well known for their good performances at room temperature and temperatures below 50 °C, whereas a strong capacity fading is reported for storage and/or cycling at elevated temperatures of 50-90 °C [11]. Several factors might limit the calendar life of the lithium-ion battery at these temperatures. It can be due to the electrode active material instability caused by the dissolution of transition metal in the electrolyte. This dissolution process does not involve changes in the bulk material but implies a degradation of the first surface layers of a positive electrode, which reduces surface diffusion pathways and leads to an increase in charge-transfer resistance [12,13]. Changes in temperature directly affect the discharge performance and discharge capacity of a lithium-ion battery [13,14]. When the temperature increases, the internal resistance of the battery decreases, the electrochemical reaction rate slows up, the internal polarization resistance decreases rapidly, and the discharge capacity and discharge platform increase. High temperatures can accelerate the migration rate of lithium ions [14]. Among all environmental factors, the temperature has the greatest impact on the charge and discharge performance of lithium-ion batteries.

Currently, many investigations are oriented to the study of the performance of cells operated at higher temperatures. Bodenes *et al*. [15] have found a good performance of $LiNi_{1-x-y}Mn_xCo_yO_2$ cells when cycled at 85 °C compared to room temperature and attributed it to the formation and thickness of the passivation layer at the positive electrode surface. Idemoto *et al*. [5] using $0.4Li_2MnO_3$-$0.6LiMn_{1/3}Ni_{1/3}Co_{1/3}O_2$ electrodes operating at 60 °C, found a capacity higher than 280 mAh $g^{-1}$ [5]. Also, Lee *et al*. [16], using $Li[Ni_{0.5}Co_{0.2}Mn_{0.3}]O_2$ and $Li[Ni_{0.6}Co_{0.2}Mn_{0.2}]$, found a significant thermal stabilizing effect of vinylene carbonate as Ni content increased, due to the formation of a thermally stable layer on the electrode surface. Temperature is considered to be an important indicator that affects the capacity of lithium-ion batteries. Therefore, it is of great significance to study the relationship between the capacity and operating temperature of lithium-ion batteries. That is why in this work, the aim was to evaluate the influence of elevated temperature operating conditions (55°C) on cells composed of LMO as the positive electrode and to compare the obtained results with those previously measured at 25 °C [17]. In addition, structural and morphological characterizations of prepared cathode materials were made by X-ray diffraction (XRD) and scanning electron microscopy (SEM).

## Experimental

### *Synthesis of $xLi_2MnO_3$-(1-x)$LiNi_{0.5}Mn_{0.5}O_2$ cathode material*

Synthesis of the cathodic material was carried out following the co-precipitation method shown by Nazario-Naveda *et al.* [17]. 0.2 M of nickel (II) sulphate hexahydrate [$NiSO_4 \cdot 6H_2O$] (Sigma-Aldrich 99 %) and 0.2 M of manganese (II) sulphate monohydrate [$MnSO_4 \cdot H_2O$] (Sigma-Aldrich 98 %) were separately dissolved in distilled water, and then mixed through 10 minutes at constant stirring. Separately a solution of 1 M of sodium bicarbonate [$NaHCO_3$] (Sigma-Aldrich 99 %) in distilled water was prepared. The first solution was slowly added drop by drop into the second one at constant magnetic stirring and a temperature of 60 °C. The mixed solution was kept at a pH of 8.5 in order to get the precipitated $Ni_{(1-x)/2}Mn_{(1+x)/2}CO_3$, and pH was controlled with drop-by-drop addition of ammonium hydroxide solution [$NH_4OH$] (Sigma Aldrich 28-30 %). The obtained mixture was left for 12 hours at the same temperature and with constant magnetic stirring in order to get a complete reaction. After that, the mixture was filtered and washed three times with distilled water. The resulting wet powder was dried for 12 hours at 100 °C and then grounded with a mortar and pestle to get nickel manganese carbonate final precursor powder. The powder was mixed with a stoichiometric amount of lithium carbonate [$Li_2CO_3$] (Strem Chemicals 99.999 %) and grounded using a mortar and pestle. After intense grinding, the mixture was annealed at 950 °C for 12 hours, and for this purpose a 15.24 cm W x 15.24 cm D x 15.24 cm H Kerr 666 furnace was used. After 12 hours, the calcined powder was quenched at room temperature to keep the oxidation states of transition metals at $4^+$ and $2^+$ for Mn and Ni, respectively. The calcined powder was ground again to obtain the $xLi_2MnO_3$-(1-x)$LiNi_{0.5}Mn_{0.5}O_2$ final powder. The quantities of $NiSO_4 \cdot 6H_2O$ and $MnSO_4 \cdot H_2O$ were varied stoichiometrically depending on the x value of $xLi_2MnO_3$-(1-x)$LiNi_{0.5}Mn_{0.5}O_2$ final cathode material powder.

### *Electrochemical coin cell fabrication*

Coin type cells (CR2032) were assembled inside the argon-filled MBraun glove box. Cathode material was prepared using 80 wt.% of $xLi_2MnO_3$-(1-x)$LiNi_{0.5}Mn_{0.5}O_2$ powder, 10 wt.% of carbon black and 10 wt.% of polyvinylidene fluoride. A slurry of the mixed powders was made by using N-methyl-2-pyrrolidinone. The aluminum foil (Alfa Aesar 99.999 %) with 0.025 mm of thickness was covered by a slurry, and the coated aluminum foil was put in a furnace at 100 °C for 12 hours and cut in small circles. For the anode, Li foil with 0.75 mm of thickness (Sigma Aldrich 99.9 %) was used, and the separator was a polypropylene membrane (Celgard 2500) with 25 µm of thickness. $LiPF_6$ dissolved in ethylene carbonate (EC) and dimethyl carbonate (DMC) in 1:2 volume ratio was used as the electrolyte.

### *Characterization techniques*

X-ray diffraction (XRD) patterns of the cathode material powder were obtained using Siemens D5000 X-ray diffractometer with Cu Kα radiation (0.15405 nm in the $2\theta$ angle range from 15 to 75° with a step of 0.02°. Morphological properties of the material were studied using a scanning electron microscope (SEM), and the analysis was conducted with JEOL 7600 FESEM system interfaced to a Thermo-Electron System Microanalysis Systems. Samples were adhered to the top of the sample holder with double-sided conductive tape, and for better resolution, Au coating was applied. The electrochemical measurements were evaluated at a 0.05, 0.10 and 0.15 C current rates between 2.5 - 4.7 V (1 C = 300 mA $g^{-1}$) using a Gamry Instruments G/PC14 potentiostat system. The C-rate was calculated using the weight of the active material and the capacity of the electrode.

## Results and discussion

X-ray diffraction patterns of $xLi_2MnO_3$-(1-x)$LiNi_{0.5}Mn_{0.5}O_2$ (x = 0.3, 0.5 and 0.7) synthesized materials are presented in Figure 1(a), which shows typical peaks in good agreement with the R3m space group related to the rhombohedral type structure for $LiMO_2$ [18]. The low-intensity peaks between 20 and 30° show characteristic peaks of the monoclinic phase with space group C2/m associated with layered composite material $Li_2MnO_3$ [19,20]. XRD patterns confirm the superlattice phase corresponding to $Li_2MnO_3$, and it becomes more notorious when the fraction of $Li_2MnO_3$ layered material is incremented in $xLi_2MnO_3$–(1-x)$LiMO_2$. The presence of small peaks (110), (020), (-111) and (021) is related to the existence of superstructure caused by the reordering of Li and Mn in the main structure, where lithium ions enter into the transition metal layers positions as expected [19,20,27]. Furthermore, the presence of (006) and (012) peaks confirm the successful formation of a well crystalline layered structure with no spinal structure using the co-precipitation synthesis method for all values of x [21].

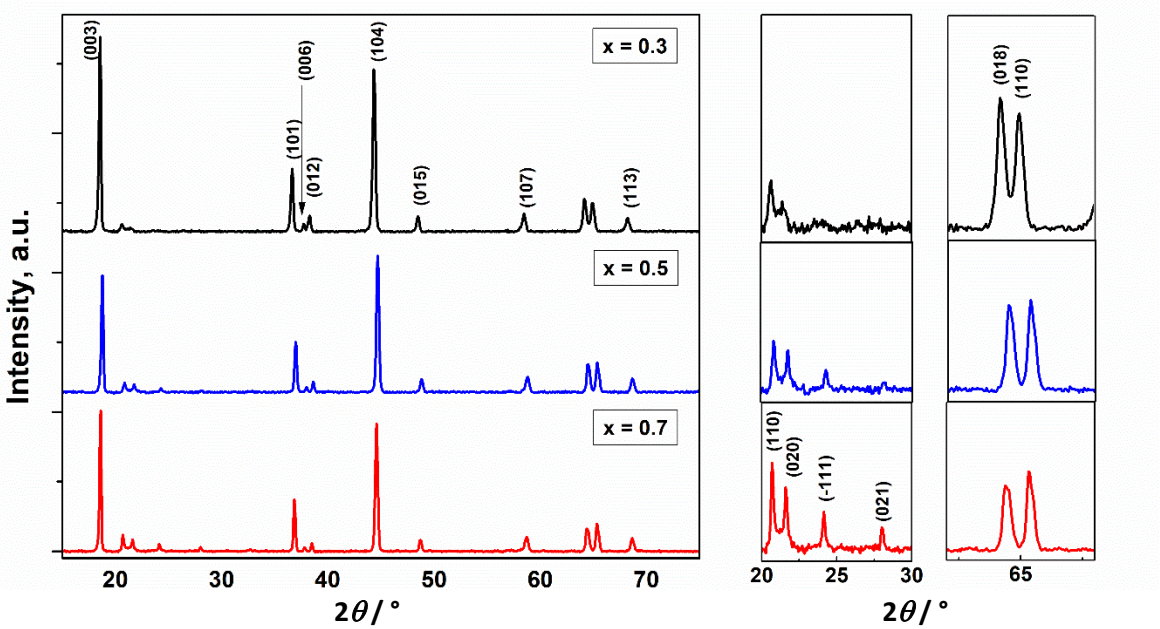


***Figure 1.*** *X-ray diffraction patterns of $xLi_2MnO_3$–(1-x)$LiNi_{0.5}Mn_{0.5}O_2$*

Scanning electron microscopy (SEM) was used to verify the morphology and topology of the synthesized material. Micrographs of synthesized $xLi_2MnO_3$–(1-x)$LiNi_{0.5}Mn_{0.5}O_2$ (x = 0.3, 0.5 and 0.7) final powders are showed in Figure 2. The primary particles are micrometric in size and concentrated in irregularly shaped agglomerations. The size of these agglomerations increases with the increase of x, and for x = 0.7, particles exceed a micrometer in length. Micrographs also show free space between agglomerations giving a high material porosity, which is good for the ions and electrons' mobility [22-24]. Relatively smaller primary particle agglomerates allow better charge/discharge capacity due to their higher trap density which shortens lithium diffusion [25]. EDS spectra shown in Figure 3 confirm the presence of respective elements in the composite materials, where intensity represents the proportions of the materials used to make the precursor materials. It is also observed that with increasing x, Ni decreases and Mn increases according to the stoichiometric proportions. Also, the presence of oxygen is increased considerably due to the predominance of the $Li_2MnO_3$ layer.

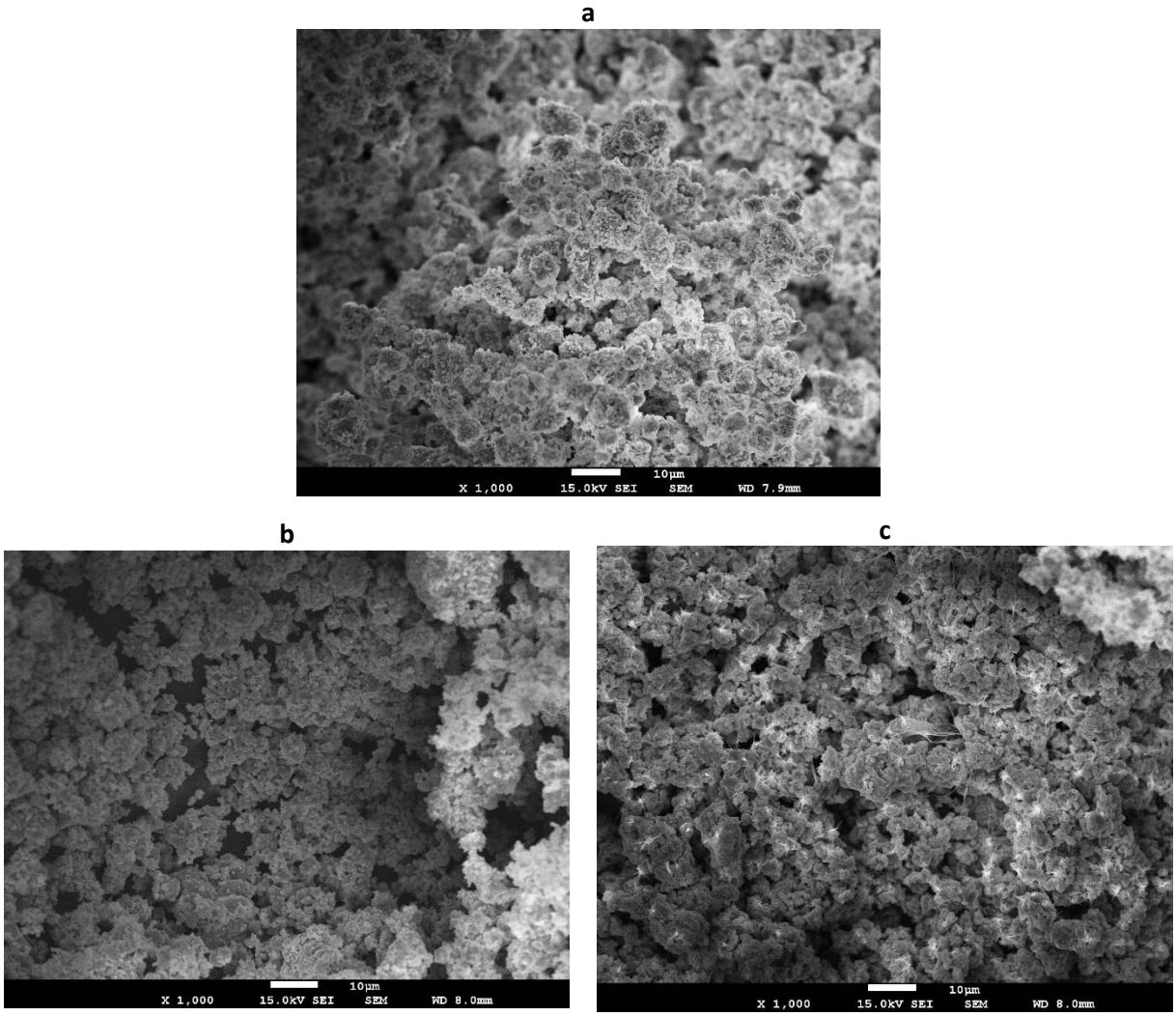


***Figure 2.*** *SEM micrographs of cathode material powders: (a) 0.3$Li_2MnO_3$–0.7$LiNi_{0.5}Mn_{0.5}O_2$, (b) 0.5$Li_2MnO_3$– 0.5$LiNi_{0.5}Mn_{0.5}O_2$, and (c) 0.7$Li_2MnO_3$–0.3$LiNi_{0.5}Mn_{0.5}O_2$*

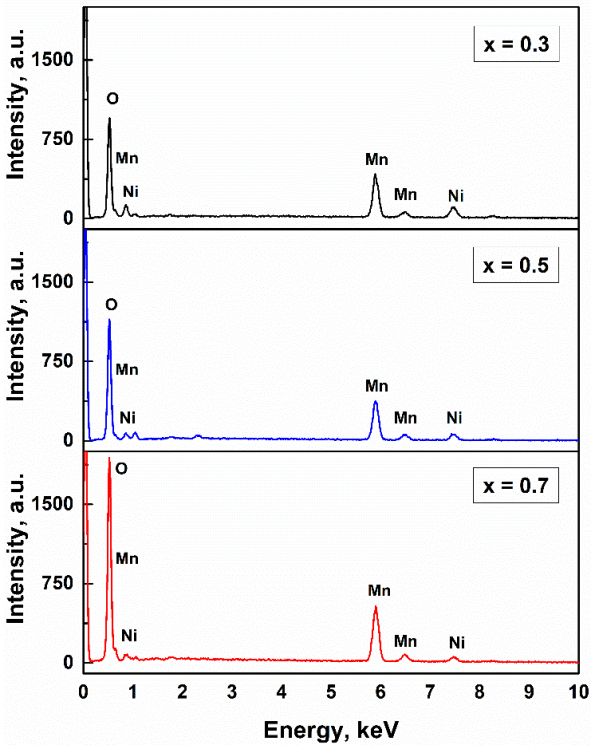


***Figure 3.*** *EDS spectra of $xLi_2MnO_{3}$-$(1-x)LiNi_{0.5}Mn_{0.5}O_2$ cathode material powders*

The electrochemical behavior of the composite at 25 °C (room temperature) and 55 °C are presented in Figures 4 and 5. Previous investigations showed that at elevated temperatures, $Li_2MnO_3$ activation is more effective than at room temperature, showing capacity values over their theoretical ones [11]. This may be due to more activation of Li ions in composite and less irreversible capacity, but the causes of this behavior are still under study. In this work, the coin cell was tested at different current densities at 55 °C after 20 cycles, *i.e.*, after the first activation and when capacity is almost constant.

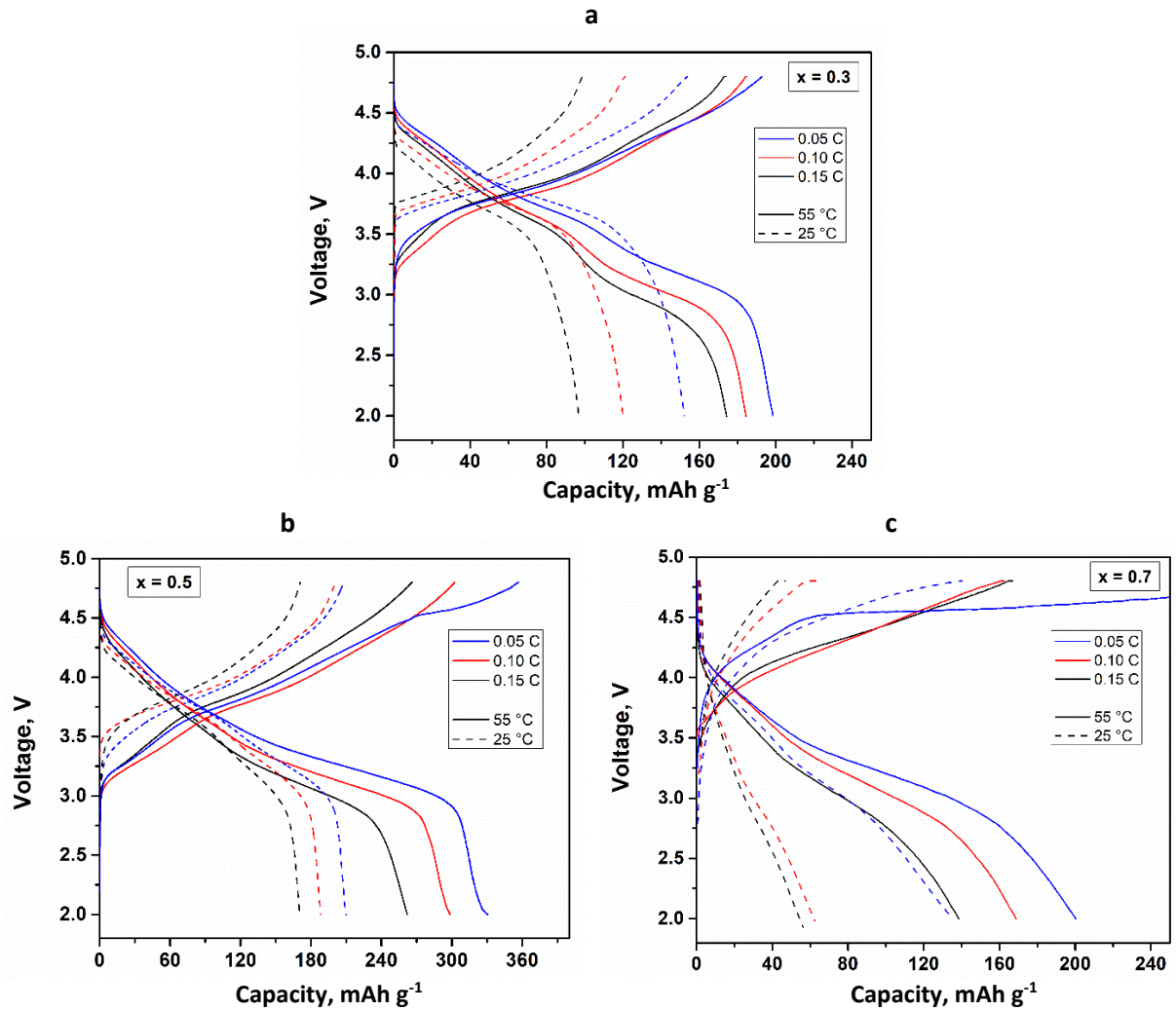


***Figure 4.*** *Charge-discharge profiles during 20th cycle at different C-rate of the LMO/Li coin cells: (a) $0.3Li_2MnO_3$–$0.7LiNi_{0.5}Mn_{0.5}O_2$, (b) $0.5Li_2MnO_3$–$0.5LiNi_{0.5}Mn_{0.5}O_2$ and (c) $0.7Li_2MnO_3$–$0.3LiNi0.5Mn_{0.5}O_2$ cycled between 2 and 4.8 V at 25 and 55 °C. Data at 25 °C are taken and adapted from ref. [17]*

Results of charge-discharge for $0.3Li_2MnO_3$–$0.7LiNi_{0.5}Mn_{0.5}O_2$ cathode material coin cells operating at different current densities are shown in Figure 4a. At room temperature, the capacity is reduced from ~150 mAh $g^{-1}$ (0.05C) to ~120 mAh $g^{-1}$ (0.10C) and ~100 mAh $g^{-1}$ (0.15C). There is a plateau voltage between 4 - 4.5 V corresponding to the Li extraction from the $LiMO_2$ component and the Li extraction from the $Li_2MnO_3$ component starts from ~4.5 V. At 55 °C, a longer activation plateau is observed. Activation is done after ~4.2 V and capacities due to the $LiMO_2$ component are higher than those at room temperature. For 0.05 C, a capacity of 200 mAh $g^{-1}$ could be reached, which is higher than the theoretical value of 196 mAh $g^{-1}$. Figure 4a also shows a spinel phase assigned plateau below 3.25 V at the discharge process of $0.3Li_2MnO_3$-$0.7LiNi_{0.5}Mn_{0.5}O_2$ electrode. This change from layered to spinel phase transformation is responsible for reducing capacities at

high cycle numbers due to the migration of transition metal ions to Li sites without high disarrange of the main layered structure, which is one of the limitations of the prolonged operation of this material at high temperatures [26].

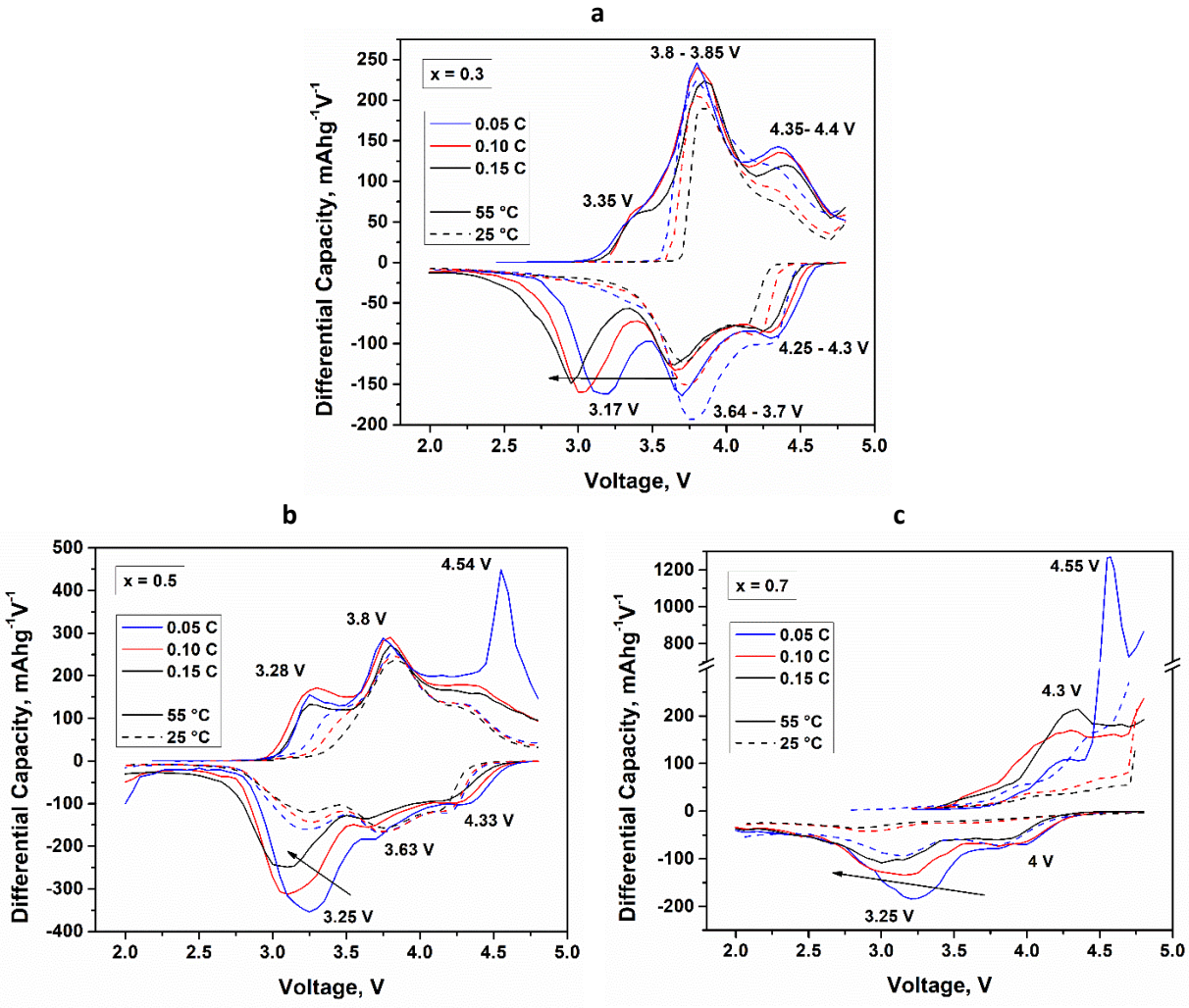


***Figure 5.*** *Differential capacity plots during 20th cycle at different C-rate of the LMO/Li coin cells (a) 0.3$Li_2MnO_3$–0.7$LiNi_{0.5}Mn_{0.5}O_2$, (b) 0.5$Li_2MnO_3$–0.5$LiNi_{0.5}Mn_{0.5}O_2$ and (c) 0.7$Li_2MnO_3$–0.3$LiNi_{0.5}Mn_{0.5}O_2$ cycled between 2 and 4.8 V at 25 and 55 °C. Data at 25 °C are taken and adapted from ref. [17]*

Figure 4b shows 0.5$Li_2MnO_3$–0.5$LiNi_{0.5}Mn_{0.5}O_2$ cathode material results. The two activation steps of this material are observed at room temperature, a first step (2-4.5 V) related to the Li extraction from $LiMO_2$ and a second step (4.5 V) due to the activation of the $Li_2MnO_3$ component. The achieved capacities were ~210 mAh $g^{-1}$ (0.05 C), ~190 mAh $g^{-1}$ (0.10 C), and ~170 mAh $g^{-1}$ (0.15 C), which are significantly below theoretical values, revealing that not all $Li_2MnO_3$ material could be activated at this current density [18]. On the other hand, at 55 °C, a new $Li_2MnO_3$ activation is shown after 4.5 V, and capacity increased from 266 to 357 mAh $g^{-1}$, contributing thus with 91 mAh $g^{-1}$. This means that at room temperature, all $Li_2MnO_3$ component is not activated, the temperature increase contributes to its activation, which doesn't occur at higher current density. Discharge capacity raised to 330 mAh $g^{-1}$, which is higher than found by other authors [15,16,26].

Figure 4c shows results for x = 0.7 cathode materials. At room temperature, differential capacity values are very low, indicating an inefficient charge transfer process between the material and the electrolyte, possibly due to the size of the conglomerates that form the material [27]. The achieved capacities were ~140 mAh $g^{-1}$ (0.05 C), ~64 mAh $g^{-1}$ (0.10 C), and ~57 mAh $g^{-1}$ (0.15 C). At 55 °C, an

activation related to Li extraction of the $Li_2MnO_3$ layer is observed, and a maximum capacity of ~200 mAh $g^{-1}$ is reached at 0.05 C, despite no observed changes to the spinel structure as observed for x = 0.3. $Li_2MnO_3$ shows to be electrochemical active at high temperatures, possibly due to low impedance, making easy $Li^+$ intercalation [5].

Figure 5 shows differential capacity plots of (a) $0.3Li_2MnO_3$-$0.7LiNi_{0.5}Mn_{0.5}O_2$, (b) $0.5Li_2MnO_3$-$0.5LiNi_{0.5}Mn_{0.5}O_2$ and (c) $0.7Li_2MnO_3$-$0.3LiNi_{0.5}Mn_{0.5}O_2$ cathode materials in coin cells operating at different C-rates of 0.05, 0.10 and 0.15 C. Differential capacities at room temperature show peaks which decrease in their intensities with an increase of the current density, and also, a degradation of the voltage when the current density increases [28,29]. These reductions in electrochemical performance could be explained considering that at high current densities, the amount of lithium insertion/extraction is affected by the structure of the interface, not allowing Li ions to leave their sites, resulting in low capacities [30]. For example, for x = 0.5 (Figure 5b), the Mn oxidation from $M^{3+}$ to $Mn^{4+}$ at ~3.4 V is only seen at 0.05 C in the charging process, but not at 0.15 C. At 55 °C, Figure 5 shows the main redox peaks of Ni and Mn for electrode material. According to the research results, a change in valence during charging and discharging based on a shift in the position of peaks associated with Mn and Ni can be observed at high temperatures. For x = 0.3 (Figure 5a) oxidation peaks appear at 3.35 V and 3.8 V for Mn and Ni oxidation respectively. Ni reduction peak appears at 3.7 V at 0.05 C and is slightly shifted to 3.64 V. On the other hand, the Mn reduction peak appears at 3.17 V at 0.05 C but quickly decreases to 2.95 V at 0.15 C, showing the same layered to spinel phase transformation tendency [31]. For x = 0.5 sharp activation peak appears at 4.54 V. Standard oxidation peaks for Ni and Mn appear at 3.8 and 3.28 V, respectively. Ni reduction peak at 3.63 V, and Mn reduction peak goes from 3.25 V at 0.05 C to 3.11 V at 0.15 C, conserving the layered-layered structure, suggesting a relatively more stable and efficient SEI film would form at 55 °C [16]. Figure 5c shows peaks of oxidation and reduction related to Ni and Mn reactions appearing for x = 0.7 but shifted to the higher voltage in the charging process and to the lower in the discharge process, indicating the formation of spinel structure [32,33]. In all cases, differential capacity values are very low, indicating an inefficient charge transfer process between the material and the electrolyte, possibly due to the size of the conglomerates that form the material [34].

## Conclusions

In this work $xLi_2MnO_3$-$(1-x)LiNi_{0.5}Mn_{0.5}O_2$ layered composite materials for x = 0.3, 0.5 and 0.7 were synthesized by carbonate assisted co-precipitation method. X-ray diffraction patterns confirmed the formation of two phases of layered crystal structure. CR2032 coin cells were successfully assembled in Ar filled glove box in order to test the electrochemical behavior of the synthesized electrode materials at 25 and 55 °C. Electrochemical results showed that at 55 °C, a change in valence could be observed during charging and discharging due to the change in the position of the peaks associated with Mn and Ni on differential capacity plots. The cells with the cathodic material with x = 0.5 presented greater stability, achieving the capacity of more than 357 mAh $g^{-1}$ at a voltage of 2.5 - 4.8 V *vs*. $Li/Li^+$, which was larger than the capacity at room temperature. Thus, the operating temperature can have a large effect on the behavior of especially Ni, which can influence the battery characteristics. Other materials (x = 0.3 and 0.7) present spinel phase formation within the structure at higher temperatures, reflected in a slow diffusion rate, inefficient $Li_2MnO_3$ activation and low capacities.

## References


[1] S. Ghosh, U. Bhattacharjee, S. Bhowmik, S. K. Martha, *Journal of Energy and Power Technology* **4(1)** (2022) 002. http://dx.doi.org/10.21926/jept.2201002

[2] J. Klink, A. Hebenbrock, J. Grabow, N. Orazov, U. Nylén, R. Benger, H.-P. Beck, *Batteries* **8(4)** (2022) 34. https://doi.org/10.3390/batteries8040034

[3] B. R. Long, J. R. Croy, F. Dogan, M. R. Suchomel, B. Key, J. Wen, D. J. Miller, M. M. Thackeray, M. Balasubramanian, *Chemistry of Materials* **26(11)** (2014) 3565-3572. https://doi.org/10.1021/cm501229t

[4] Y. Yang, X. Huang, Z. Cao, G. Chen, *Nano Energy* **22** (2016) 301-309. http://dx.doi.org/10.1016/j.nanoen.2016.01.026

[5] Y. Idemoto, T. Hiranuma, N. Ishida, N. Kitamura, *Journal of Power Sources* **378** (2018) 198-208. https://doi.org/10.1016/j.jpowsour.2017.12.045

[6] S. S. Nisa, M. Rahmawati, C. S. Yudha, H. Nilasary, H. Nursukatmo, H. S. Oktaviano, H. S. Muzayanha, A. Purwanto, *Batteries* **8** (2022) 4. https://doi.org/10.3390/batteries8010004

[7] B. Xu, D. Qian, Z. Wang, Y. S. Meng, *Materials Science and Engineering R: Reports* **73(5-6)** (2012) 51-65. http://dx.doi.org/10.1016/j.mser.2012.05.003

[8] H. Yu, H. Zhou, *Journal of Physical Chemistry Letters* **4(8)** (2013) 1268-1280. https://doi.org/10.1021/jz400032v

[9] H. Konishi, T. Hirano, D. Takamatsu, A. Gunji, X. Feng, S. Furutsuki, T. Okumura, S. Terada, *Solid State Ionics* **308** (2017) 84-89. https://doi.org/10.1016/j.ssi.2017.06.005

[10] D. Kim, G. Sandi, J. R. Croy, K.G. Gallagher, S.-H. Kang, E. Lee, M. D. Slater, C. S. Johnson, M. M. Thackeray, *Journal of The Electrochemical Society* **160(1)** (2013) A31-A38. https://doi.org/10.1149/2.049301jes

[11] L. Madec, G. Gachot, G. Coquil, H. Martinez, L. Monconduit, *Journal of Power Sources* **391** (2018) 51-58. https://doi.org/10.1016/j.jpowsour.2018.04.068

[12] A. Samanta, S. S. Williamson, *Energies* **14(18)** (2021) 5960. https://doi.org/10.3390/en14185960

[13] S. Ma, M. Jiang, P. Tao, C. Song, J. Wu, J. Wang, T. Deng, W. Shang, *Progress in Natural Science: Materials International* **28(6)** (2018) 653-666. https://doi.org/10.1016/j.pnsc.2018.11.002

[14] H. Liu, Z. Wei, W. He, J. Zhao, *Energy Conversion and Management* **150** (2017) 304-330. https://doi.org/10.1016/j.enconman.2017.08.016

[15] L. Bodenes, R. Dedryvère, H. Martinez, F. Fischer, C. Tessier, J.-P. Pérès, *Journal of The Electrochemical Society* **159(10)** (2012) A1739. https://doi.org/10.1149/2.061210jes

[16] W. J. Lee, K. Prasanna, Y. N. Jo, K. J. Kim, H. S. Kim, C. W. Lee, *Physical Chemistry Chemical Physics* **16(32)** (2014) 17062-17071. http://dx.doi.org/10.1039/c4cp02075h

[17] R. Nazario-Naveda, S. Rojas-Flores, L. Juárez-Cortijo, M. Gallozzo-Cardenas, F. N. Díaz, L. Angelats-Silva, S. M. Benites, *Batteries* **8(7)** (2022) 63. https://doi.org/10.3390/batteries8070063

[18] H. Konishi, T. Hirano, D. Takamatsu, T. Okumura, *Journal of Electroanalytical Chemistry* **873** (2020) 114402. https://doi.org/10.1016/j.jelechem.2020.114402

[19] Y. Jiang, Z. Yang, W. Luo, X. Hu, Y. Huang, *Physical Chemistry Chemical Physics* **15(8)** (2013) 2954-2960. https://doi.org/10.1039/C2CP44394E

[20] Y. Xiang, J. Li, Q. Liao, X. Wu, *Ionics* **25(1)** (2019) 81-87. https://doi.org/10.1007/s11581-018-2569-4

[21] J. Guo, Z. Deng, S. Yan, Y. Lang, J. Gong, L. Wang, G. Liang, *Journal of Materials Science* **55(27)** (2020) 13157-13176. https://doi.org/10.1007/s10853-020-04973-0

[22] J. Wang, X. He, E. Paillard, N. Laszczynski, J. Li, S. Passerini, *Advanced Energy Materials* **6(21)** (2016) 1600906. https://doi.org/10.1002/aenm.201600906

[23] M. Gu, I. Belharouak, J. Zheng, H. Wu, J. Xiao, A. Genc, K. Amine, S. Thevuthasan, D. R. Baer, J.-G. Zhang, N. D. Browning, J. Liu, C. Wang, *ACS Nano* **7(1)** (2013) 760-767. https://doi.org/10.1021/nn305065u

[24] S. Hy, H. Liu, M. Zhang, D. Qian, B.-J. Hwang, J.S. Meng, *Energy & Environmental Science* **9(6)** (2016) 1931-1954. https://doi.org/10.1039/C5EE03573B

[25] C. Yu, G. Li, X. Guan, J. Zheng, L. Li, *Electrochimica Acta* **61** (2012) 216-224. https://doi.org/10.1016/j.electacta.2011.12.010

[26] M.-H. Ryou, G.-B. Han, Y.M. Lee, J.-N. Lee, D.J. Lee, Y.O. Yoon, J.-K. Park, *Electrochimica Acta* **55(6)** (2010) 2073-2077. https://doi.org/10.1016/j.electacta.2009.11.036

[27] K. Redel, A. Kulka, A. Plewa, J. Molenda, *Journal of The Electrochemical Society* **166(3)** (2019) A5333-A5342. https://doi.org/10.1149/2.0511903jes

[28] N. Meddings, M. Heinrich, F. Overney, J.-S. Lee, V. Ruiz, E. Napolitano, S. Seitz, G. Hinds, R. Raccichini, M. Gaberšček, J. Park, *Journal of Power Sources* **480** (2020) 228742. https://doi.org/10.1016/j.jpowsour.2020.228742

[29] Y. Nie, W. Xiao, C. Miao, M. Xu, C. Wang, *Electrochimica Acta* **334** (2020) 135654. https://doi.org/10.1016/j.electacta.2020.135654

[30] S. Zhao, K. Yan, J. Zhang, B. Sun, G. Wang, *Angewandte Chemie International Edition* **60(5)** (2021) 2208-2220. https://doi.org/10.1002/anie.202000262

[31] S. Hy, W.-N. Su, J.-M. Chen, B.-J. Hwang, *The Journal of Physical Chemistry C* **116(48)** (2012) 25242-25247. https://doi.org/10.1021/jp309313m

[32] S. Hy, H. Liu, M. Zhang, D. Qian, B.-J. Hwang, Y. S. Meng, *Energy & Environmental Science* **9(6)** (2016) 1931-1954. https://doi.org/10.1039/C5EE03573B

[33] H. Peng, S.-X. Zhao, C. Huang, L.-Q. Yu, Z.-Q. Fang, G. D. Wei, *ACS Applied Materials & Interfaces* **12(10)** (2020) 11579-11588. https://doi.org/10.1021/acsami.9b21271

[34] S. Lv, X. Wang, W. Lu, J. Zhang, H. Ni, *Energies* **15(1)** (2021) 60. https://doi.org/10.3390/en15010060